Astron. Astrophys. 348, 198–210 (1999)

ASTRONOMY AND ASTROPHYSICS

Chromospheric models for late A-type stars⋆

P. Gouttebroze[1], **R. Freire Ferrero**[2], **E. Marilli**[3], **and S. Catalano**[3]

[1] Institut d'Astrophysique Spatiale, Unité Mixte CNRS-Université Paris XI, bât 121, F-91405 Orsay Cedex, France
[2] Observatoire Astronomique, 11 rue de l'Université, F-67000 Strasbourg, France
[3] Osservatorio Astrofisico di Catania, Viale A. Doria 6, I-95125 Catania, Italy

Received 29 May 1997 / Accepted 21 May 1999

Abstract. The chromospheres of α Aql (Altair) and α Cep (Alderamin) are investigated. Different semi-empirical model atmospheres are constructed, and the predicted spectra are compared to the observations of the hydrogen Lyman-α line (IUE) and carbon (both neutral and ionized) multiplets (GHRS-HST). It is found that chromospheric models at low temperature ($\sim$ 10000 K) which fit the Lα line, produce C II lines in absorption, contrary to observations. Among the models investigated, only those with a mean temperature of $\sim$ 20000 K are able to fit simultaneously the Lα and C II lines. Provisional reference models are proposed for α Aql. The lower emission of α Cep with respect to α Aql is better explained by a difference of column mass than by a difference of temperature. The chromospheric column mass ratio (α Cep / α Aql) is estimated to about 0.8. For both stars, the relatively narrow dips of the C II emission feature cannot be of stellar origin, owing to the fast rotation, but of interstellar absorption nature.

Key words: line: profiles – stars: atmospheres – stars: chromospheres – stars: Hertzsprung–Russel (HR) and C-M diagrams – ISM: atoms, ions

1. Introduction

It seems now well established that the existence of chromospheric layers in stars is due to the deposition of nonthermal energy produced in an underlying convective zone. Classical theories of stellar convection predict that these convective zones become shallow and may disappear at middle A-type stars. For these reasons, it is very important to study how chromospheric structures vary near the region separating stars with and without external convective zones in the H-R diagram. Chromospheres have been found until the A7 stellar type by detection of hydrogen Lyman-α line core emission, the most sensitive chromospheric indicator for this spectral type: α Aql (A7 V, Blanco et al. 1980, Freire Ferrero et al. 1990, Catalano et al. 1990, 1991), γ Boo (A7 III, Marilli et al. 1992), α Cep (A7 IV-V) and ι UMa (A7 IV) (Freire Ferrero et al. 1992, Marilli et al. 1997).

Chromosphere modelling techniques and possible models for α Aql have been discussed by Freire Ferrero et al. (1995, hereafter FF95). Several models were tested, having chromospheric temperature rises ranging from 9000 to 20000 K; some of them give very good profile fitting to the observed emission, at the expense, however, of some increase of the apparent rotational velocity for the hottest models.

In the meantime, Simon et al. (1994) searched for chromospheric emissions in the C II resonance doublet, near 1335 Å in several A stars by using the Goddard High Resolution Spectrograph on board of the Hubble Space Telescope. They detected C II emission in α Aql. Walter et al. (1995) subsequently observed and analyzed α Aql and α Cep in the same spectral region. They concluded that α Cep also shows C II chromospheric emission.

The existence of chromospheric emission in two different spectral features (Lα and C II lines) brings an opportunity to refine the chromospheric models of α Aql and α Cep, because no other classical UV chromospheric indicator is seen in these stars (namely Mg II h and k lines, cf. FF95). In the following, we model chromospheres for these two stars using the simultaneous constraints to fit both observed Lα and C II emissions. To this purpose, we use the Lα observations of Marilli et al. (1997). The C I and C II observations are taken from the HST database and averaged over intervals of ± 0.1 Å in order to reduce the noise. For α Aql, we use an average of the spectra given by Simon et al. (1994) and Walter et al. (1995). For α Cep, we use the spectrum given by Simon et al. (1994).

2. Numerical methods

2.1. Computations of structure and hydrogen spectrum

The stellar atmosphere models are defined by the surface gravity, the abundance of the principal elements, and the variations of temperature and microturbulent velocity as functions of column mass. The numerical code HYDR computes the other physical parameters (pressure, electron density, altitudes, etc.) as well as the hydrogen spectrum (lines and continua). It solves simul-

Send offprint requests to: P. Gouttebroze

⋆ Based on observations by the IUE satellite collected at Villafranca ESA IUE Observatory and at the GSFC NASA IUE Observatory. Also based on observations made with the NASA/ESA Hubble Space Telescope, obtained from the data archive, at the Space Telescope Science Institute, which is operated by the Association of Universities for Research in Astronomy, Inc., under contract NAS 5-26555.

taneously the equations of hydrostatic equilibrium, ionization, statistical equilibrium of hydrogen level populations, and radiative transfer in lines and continua of hydrogen. Other chemical constituents are treated in LTE.

Radiative transfer in each transition is solved by the Feautrier method with variable Eddington factors. Other equations are solved by iteration. The hydrogen atom model includes 20 levels and one continuum. Non-LTE radiative transfer is explicitly solved for the 10 principal lines (whose upper level is lower than 6). Other lines are assumed in radiative balance. Standard partial redistribution is used for Lα and Lβ, while complete redistribution is assumed for the 8 other lines (partial redistribution is treated as described in FF95).

For the hydrogen lines, the spontaneous transition probabilities and the collisional excitation rates are calculated with the formulae of Johnson (1972). For continua, we use the collisional ionization rates of Clark et al. (1991). Collisional broadening of lines is specified according to Sutton (1978) for Stark broadening and Lortet & Roueff (1969) for combined resonance and Van der Waals broadening.

2.2. Comparison of the computed Lyman-α profiles with observations

Once the Lα intensities are computed for different frequencies and angle of emergence, several operations are necessary to perform the comparison with observations:

- The intrisic flux of the star is obtained by integrating the intensities coming from the different regions of the stellar disk, taking into account the Doppler shifts due to the rotation. Owing to the lack of information concerning an eventual differential rotation, the star is assumed to rotate as a rigid body.
- The spectrum is shifted in frequency to account for the radial velocity of the star.
- The intrinsic flux is converted to flux at earth by multiplying it by $(R/d)^2$, where R is the radius of the star and d the star-to-earth distance.
- Since the center of the line is contaminated by interstellar (IS) hydrogen, it is also necessary to specify a model for this IS absorption. For the stars under consideration, the IS absorption feature is highly saturated. As a consequence, it may be treated as a Lorentz profile and the model of IS absorption reduces to 2 parameters: the number of hydrogen atoms per unit area along the line of sight, and the radial velocity of the IS cloud. These two quantities may be determined by trial and error.
- Finally, as the observed spectrum is smoothed (in order to reduce noise) over a bandpass of 0.26 Å, we apply the same smoothing to the computed flux.

2.3. Carbon lines

To compute the three multiplets (C I 1329 Å, C II 1335 and 1324 Å), we use a simplified model of carbon atom containing only the relevant levels for the transitions under consideration, i. e. 6 multiple levels with 13 sublevels. Level 1 is the fundamental of C I ($2p^2\ ^3P$) and contains 3 sublevels. Level 2 is an excited level of C I ($2p^3\ ^3P^0$) with 3 sublevels. Level 3 is the fundamental of C II ($2p\ ^2P^0$) with 2 sublevels. Levels 4 and 5 are excited levels of C II ($2p^2\ ^2D$ and $2p^3\ ^2D$) with 2 sublevels each. Finally, level 6 is the fundamental of C III (1 sublevel).

The C I multiplet (1329 Å) takes place between levels 1 and 2 and contains 6 permitted subtransitions. The principal multiplet of C II (1335 Å) corresponds to levels 3 and 4 and contains 3 permitted subtransitions. The weaker C II multiplet (1324 Å) corresponds to levels 4 and 5 and contains 4 permitted subtransitions.

We apply to these multiplets a non-LTE radiative transfer technique which takes into account the fine structure and treats, in a simplified way, the effects of partial redistribution (except for 1324 Å, which is treated in complete redistribution). This method assumes, however, that the sublevels are populated in a regular way, i.e. proportionally to their statistical weights (see Appendix). An advantage of the method is that the computation of statistical equilibrium includes the 6 global levels only, so that the convergence is very fast.

For the C I multiplet, we use the transition probabilities of Wiese et al. (1966), while the collisional excitation cross-sections and collisional broadening parameters come from Vernazza et al. (1981). For the C II multiplet at 1335 Å, we first used the atomic parameters of Lites et al. (1978). However, computations made with different stellar models (in particular solar ones) yield a ratio of the red to the blue component of this multiplet which did not agree with observations. So, we decided to correct empirically the transition probabilities for this multiplet, as explained below.

Photoionization cross-sections for both C I and C II are taken from the Opacity Project database TOPbase (Cunto et al. 1993). The photoionization rates are determined using a 2-dimension (depth and wavelength) table of intensities previously computed by HYDR.

The carbon-to-hydrogen abundance ratio is taken as 3×10^{-4}, a value intermediate between those found for Vega (2.2×10^{-4}) and for the Sun (3.8×10^{-4}) by Stürenburg & Holweger (1990).

2.4. Empirical correction of transition probabilities

The triplet of C II near 1335 Å looks like a doublet, with a blue component at 1334.53 Å and a red component formed by two lines at 1335.66 and 1335.71 Å, respectively. We computed these lines for the solar model "C" of Vernazza et al. (1981), with the transition probabilities of Lites et al. (1978). These lines are completely in emission in the solar case, the peak intensities being higher than the continuum by two orders of magnitude. The integrated intensity of the red component so obtained was about two times higher than that of the blue component. Then, we compared this result with observations of the solar spectrum obtained with the SUMER spectrometer aboard the SOHO solar observatory (Lemaire 1998, priv. comm.). The ratio of inte-

Table 1. Empirical correction of radiative transition probabilities (a) wavelength (Å), statistical weights, and transition probabilities (b) ratios (red/blue) of integrated intensities
(obs = observations SOHO/SUMER; LSC = Lites et al. 1978; cor = with corrected rates)

λ	g_l	g_u	$(A_{ul})_{LSC}$	$(A_{ul})_{cor}$
1334.53	2	4	2.06(+8)	2.6(+8)
1335.66	4	4	4.3(+7)	4.0(+7)
1335.71	4	6	2.55(+8)	2.2(+8)
		$(I_r/I_b)_{obs}$	$(I_r/I_b)_{LSC}$	$(I_r/I_b)_{cor}$
		1.39	2.05	1.43

grated intensities of the two components was in this case about 1.4. Raising the transition probability of the blue component by about 25% and lowering those of the red components in order to keep the same global transition rate, we obtain a ratio of integrated intensities similar to the observed one. This operation is summarized in Table 1. With these new transition probabilities, we also obtain a better agreement between computations and observations for α Aql.

2.5. Continua and weak lines

The computation of continuum intensities takes into account the absorptions by H (bound-free), H^-, C I, Mg I, Al I, Si I and Fe I, and the Rayleigh and Thomson scatterings. The contributions of H I, H^- and Rayleigh scattering are derived from the non-LTE hydrogen populations computed by HYDR. The contributions of metals are computed according to LTE. The photoionization cross-sections for metals are taken from Vernazza et al. (1976), and the H^- absorption coefficients from John (1988). The main contributions to the formation of the continuum appear to be the absorption by silicon and the Rayleigh scattering, due to the neighbourhood of the Lα line. There are also some contributions of carbon and, marginally, of the hydrogen Balmer continuum.

In the solar case, Vernazza et al. (1976) found important departures from LTE in the populations of neutral silicon which have some consequences on the emergent intensities in the continuum. However, the case of Altair is different, since this silicon continuum is formed in the photosphere while, in the Sun, it is formed in the temperature minimum region between photosphere and chromosphere. Thus, we may expect that the departures from LTE in the region of formation of the continuum are much weaker in the case of Altair.

The frequency interval under consideration (1320–1350 Å) is spanned by many weak lines of different elements. To compute the absorption coefficients due to these lines, we use the line list gf0140.10 of Kurucz (1998), which gives the atomic parameters for about 10000 lines between 1300 and 1400 Å. When we consider an atmospheric model without a chromosphere, we simply treat the lines in LTE, i.e. we assume that the partial source function produced by these lines is equal to the Planck function. When we add a chromosphere, this approximation is no more realistic, and there appears a large number of spurious emission lines due to the overestimation of the source function. Since it is not possible in practice to apply a full non-LTE treatment to all the elements responsible for these emissions, we adopt the following approximation: Each line is first computed in LTE and, if the line is not in emission, its source function is kept equal to the Planck function. If the line shows an emission in LTE, its source function is recomputed as for a two-level atom with complete redistribution. This computation requires, in addition to the radiative rates given by the line list, the knowledge of collisional excitation cross sections in order to solve the radiative transfer equation. To this purpose, we use the approximation of Van Regemorter (1962). After this treatment, most of the artificial LTE emission lines disappear and it remains a few emission lines with intensities compatible with observations (owing to the fast rotation, a detailed comparison of these weak emissions with observations is not possible).

As in the case of hydrogen lines, several further operations (reduction to earth flux, rotation, correction of radial velocity, IS absorption modelling) have been considered to perform the comparison with observations.

3. Models for α Aql

3.1. The (radius/distance) ratio

The angular diameter of α Aql has been measured by interferometry by Hanbury Brown et al. (1967, 1974). Combined with the distance of 5.0 pc, their result corresponds to a radius of 1.6 $R_\odot$. Another determination by Shallis & Blackwell (1980), using the infrared flux method, yields 1.82 $R_\odot$. The relation of Barnes & Evans (1976), which gives the angular diameter as a function of blue and visual magnitudes, yields, for $V = 0.77$ and $B - V = 0.22$: $(R/d) = 7.8 \times 10^{-9}$. This corresponds to a radius of $1.72 R_\odot$. This last value has the advantage to be intermediate between the two direct measurements, so that we adopt it for the present computations.

3.2. Rotation velocity

The apparent rotation velocity $v \sin i$ of α Aql has been investigated by several authors, and the values obtained seem to depend on the method and on the spectral lines used for this investigation. This effect could be due to some inconsistency between polar and equatorial regions, generated by the fast rotation: lines emanating principally from polar regions seem to indicate low rotation, while those which are stronger in equatorial regions yield apparent fast rotation (see Carpenter et al. 1984 and references therein). For α Aql, most investigations yield rotation velocities in the range 220–250 km s^{-1}. Some UV lines produce values as low as 190 km s^{-1} (Carpenter et al. 1984), while FF95 suggest values as high as 300 km s^{-1} for obtaining the best fit in Lα.

In the following, we use the mean value of 240 km s^{-1}, unless explicitly indicated.

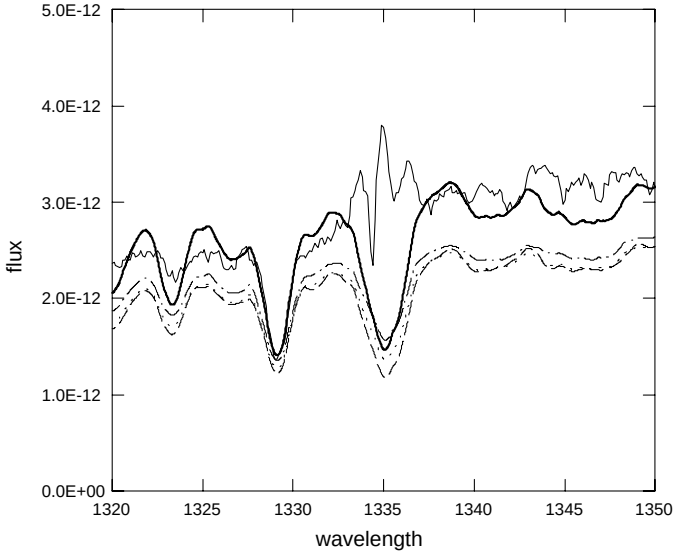

Fig. 1. Comparison of measured and computed fluxes at earth for α Aql (erg cm^{-2} s^{-1} Å^{-1}) vs. wavelength (Å), for models without chromosphere. Thin solid line: GHRS (HST) observations. Computations from Kurucz (1979) models: dashed line: (8000,3.5,0); dotted line: (8000,4.0,0); dot-dashed line: (8000,4.5,0). Thick solid line: computation with the model of Table 2 and $\log g = 4$. The rotational velocity ($v \sin i$) is 240 km s^{-1} and the radial velocity -25 km s^{-1}.

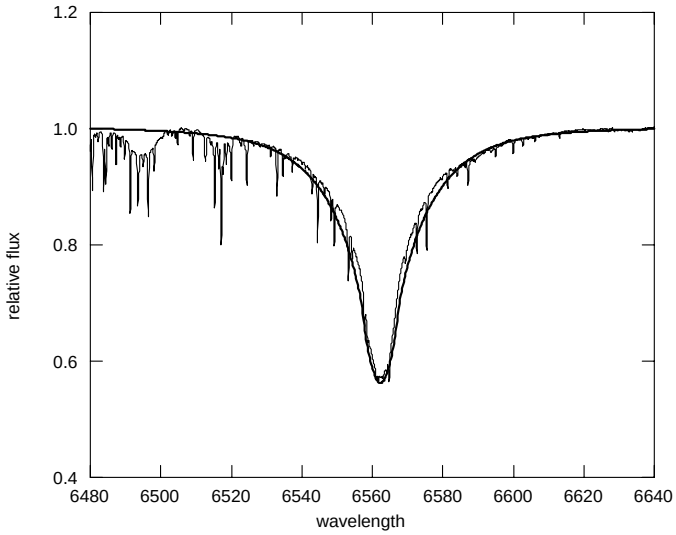

Fig. 2. Comparison of measured and computed Hα line profiles for α Aql. Thin line: observations by Lanz & Catala (1992). Thick line: computations with the model of Table 2 and $\log g = 4$. The rotational velocity ($v \sin i$) is 240 km s^{-1} and the radial velocity -25 km s^{-1}. Computed wavelengths (Å) are corrected for the refraction index of air.

3.3. Photospheric model

Estimations of the surface gravity of α Aql vary from $\log g = 3.8$ (FF95) to 4.29 (Malagnini & Morossi, 1990), while its effective temperature is close to 8000 K. The intensities in the spectral range (1320–1350 Å) have been computed with the 3 photospheric models of Kurucz (1979) corresponding to the effective temperature of 8000 K, normal abundances, and $\log g$ = 3.5, 4.0 and 4.5, respectively. No chromosphere is added: the models are linearly extrapolated outwards until the temperature reaches 5000 K. In outer layers, the temperature is assumed constant. These 3 models give very similar results, as may be seen in Fig. 1. The only noticeable difference concerns the absorption in the C II multiplet.

Table 2. Photospheric model for α Aql: temperature (K) vs. column mass ($g\,cm^{-2}$)

$\log m$	T	$\log m$	T	$\log m$	T	$\log m$	T
-7.00	5000	-1.80	5830	-0.70	6600	0.05	11400
-3.00	5000	-1.70	5900	-0.60	6680	0.10	13000
-2.89	5020	-1.60	5970	-0.50	6800	0.20	16000
-2.77	5110	-1.50	6040	-0.40	6940	0.30	18400
-2.65	5200	-1.40	6110	-0.30	7100	0.40	20400
-2.53	5290	-1.30	6180	-0.25	7200	0.50	21800
-2.41	5380	-1.20	6250	-0.20	7400	0.60	23000
-2.29	5470	-1.10	6320	-0.15	7700	0.70	24000
-2.17	5560	-1.00	6390	-0.10	8100		
-2.05	5650	-0.90	6460	-0.05	8800		
-1.93	5740	-0.80	6530	0.00	10000		

Thus, a precise determination of surface gravity does not seem to be critical in the present analysis: we adopt the mean value $\log g = 4.0$. To improve the fit, we introduce a variation of temperature vs. mass slightly hotter than that corresponding to the model (8000,4.0,0) of Kurucz (1979). This photospheric model is given in Table 2 and the resulting intensities in the spectral range (1320–1350 Å) are shown in Fig. 1. We also compared the Hα profile predicted by this model to the observations of Lanz & Catala (1992). The agreement between the computed and observed relative fluxes is good, whereas the computed profile is slightly broader than the observed one (Fig. 2). This photospheric model, complemented with different chromospheric models, will be used for the rest of the computations on α Aql.

Computed fluxes not only depend on the variation of temperature of the model with altitude, but also, to a lesser extent, on microturbulence. For the same chromospheric variation of temperature, one obtains lower emission when the microturbulent velocity is larger, for Lα as well as for the C II multiplet. Microturbulence increases the distance between the peaks of intensity and decreases their height; after application of stellar rotation, the emission flux tends to decrease.

In the case of α Aql, an independent determination of non-thermal velocities is not possible, because the rotational width is much larger than the natural width of the lines. Thus, we keep the value of 5 km s^{-1} used in FF95, which seems to be an acceptable mean value for this type of stars.

3.4. A chromospheric model with constant gradient (CG)

One of the simplest possible models for a chromosphere may be constructed by appending to the preceding photospheric model a slab where the logarithm of temperature varies linearly with the logarithm of column mass. Such a model depends on 2 param-

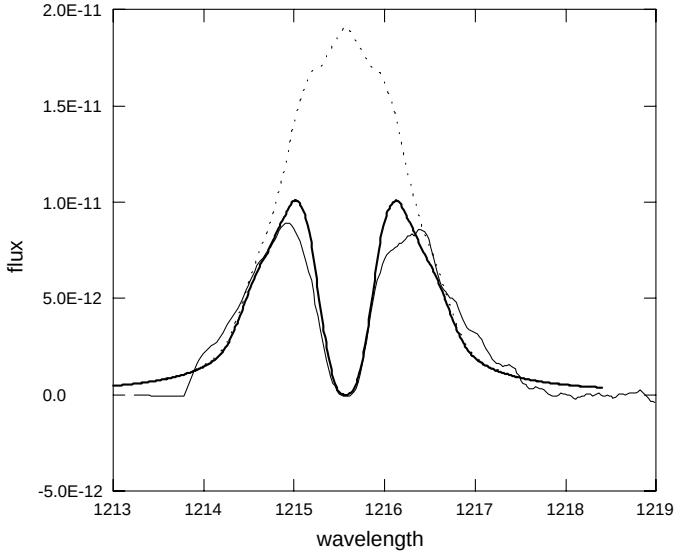

Fig. 3. Lyman-α profile emitted by model CG, compared to observations of α Aql (same units as Fig. 1). Thin line: IUE observations; dotted line: computed profile without IS absorption; thick line: the same with IS absorption.

eters only: the slope $(-d\log T/d\log m)$ and the column mass m_0 where the temperature begins to rise from the temperature minimum of 5000 K. We have found, by trial and error, that the model with $(-d\log T/d\log m) = 0.4$ and $\log m_0 = -3.6$ produces a good fit of the Lα line. This model will be hereafter referred to as "CG". The comparison of the observed and computed Lα profiles is shown in Fig. 3, for the standard rotation velocity 240 km s^{-1} and a column density of IS hydrogen: $\log n_H = 18.5$.

The profiles of carbon lines obtained with model CG are shown in Fig. 4. The C I multiplet, by the effect of rotation, produces an absorption which is practically the same as that corresponding to the model without chromosphere. On the contrary, the C II multiplet produces a rather complex profile with several dips and peaks. It may be interpreted as a chromospheric emission superimposed to a photospheric absorption. However, this chromospheric emission is not sufficient to match the observations, as may be seen in Fig. 4a. In Fig. 4b, we compare the flux computed with the standard rotation velocity to the flux obtained by setting this velocity to zero (i. e. as seen by a co-rotating observer). This figure shows how the three sharp absorption lines of the C I multiplet are transformed by the rotation into a single broad absorption feature, and how the two C II lines, with strong but narrow emission peaks surrounded by wings, may produce the complex profile of Fig. 4a. Fig. 5 shows the complete atmospheric model with the regions of formation of the line core of the two principal multiplets ($0.1 < \tau < 10^3$), and of the local continuum ($0.1 < \tau < 10$). This continuum is formed in the upper photosphere near 6500 K, the C I multiplet in the low chromosphere and C II in the upper chromosphere. While the line cores of the C I multiplet are formed in the chromosphere, they produce no emission as a result of non-LTE effects. The C II emission lines are optically thick and (in the absence of rotation) self-reversed. The red emission feature is asymmetric because it contains two different transitions. These multiplets, controlled by collisions, are relatively insensitive to photoionization rates. The collisional quenching factor ϵ varies from 10^{-7} to 10^{-5} for the C II multiplet, in its region of formation.

Since this constant gradient model is not sufficient to fit simultaneously the different lines (Lα and carbon multiplets), it is necessary to investigate less rudimentary models.

Table 3. Chromospheric models for α Aql with a temperature plateau

	P10		P15		P20		P25
$\log m$	T	$\log m$	T	$\log m$	T	$\log m$	T
-6.0	99999	-6.0	99999	-6.0	99999	-6.0	99999
-5.7	10000	-5.8	15000	-5.8	20000	-5.8	25000
-4.0	10000	-4.45	15000	-4.65	20000	-4.85	25000
-3.9	5000	-4.25	5000	-4.45	5000	-4.45	5000
-3.0	5000	-3.0	5000	-3.0	5000	-3.0	5000

3.5. Chromospheric models with temperature plateau

Another simple type of chromospheric model is that proposed in FF95. It consists of a sharp rise of temperature followed by an isothermal layer or *plateau*. The two principal parameters of the model are the temperature of the plateau and the location (in column mass units) of the temperature jump (the temperature minimum is still fixed at 5000 K). Towards external layers, the models are completed with a sharp temperature rise which reaches 10^5 K for a column mass of 10^{-6} g cm^{-2}. This rise may represent a chromosphere-corona transition region. With such a model, it is possible to study the effect of a concentration of matter at a given temperature on line profiles. FF95 found that the Lα emission in α Aql could be explained by different models with temperature plateaux ranging from 9000 to 20000 K, the thickness (in column mass units) decreasing for increasing temperatures.

Here, we investigate four models with temperature plateaux at 10000 K (model P10), 15000 K (P15), 20000 K (P20) and 25000 K (P25), respectively. In each case, the location of the temperature rise is adjusted in order to obtain the best fit for the Lα line. The temperature structure of these models is summarized in Table 3. In Figs. 6 and 7, the different profiles corresponding to the four models and the two spectral ranges are shown. For Lα (Fig. 6), a reasonable agreement is found in any case: at high temperature, the profile is slightly too narrow, but a quasi-perfect fit may be recovered by raising $v \sin i$ from 240 to 300 km s^{-1}, as pointed out by FF95 (the possible reasons of this apparent excess velocity are discussed in their paper).

On the contrary, the four models give very different profiles for the C II multiplet (Fig. 7). P10 produces an absorption feature, but somewhat shallower than that obtained without chromosphere (Fig. 7a). This means that some chromospheric emission exists, but is too weak to fill in the photospheric absorption. Model P15 produces a profile which is partly in absorption and partly in emission with respect to the continuum (Fig. 7b). This

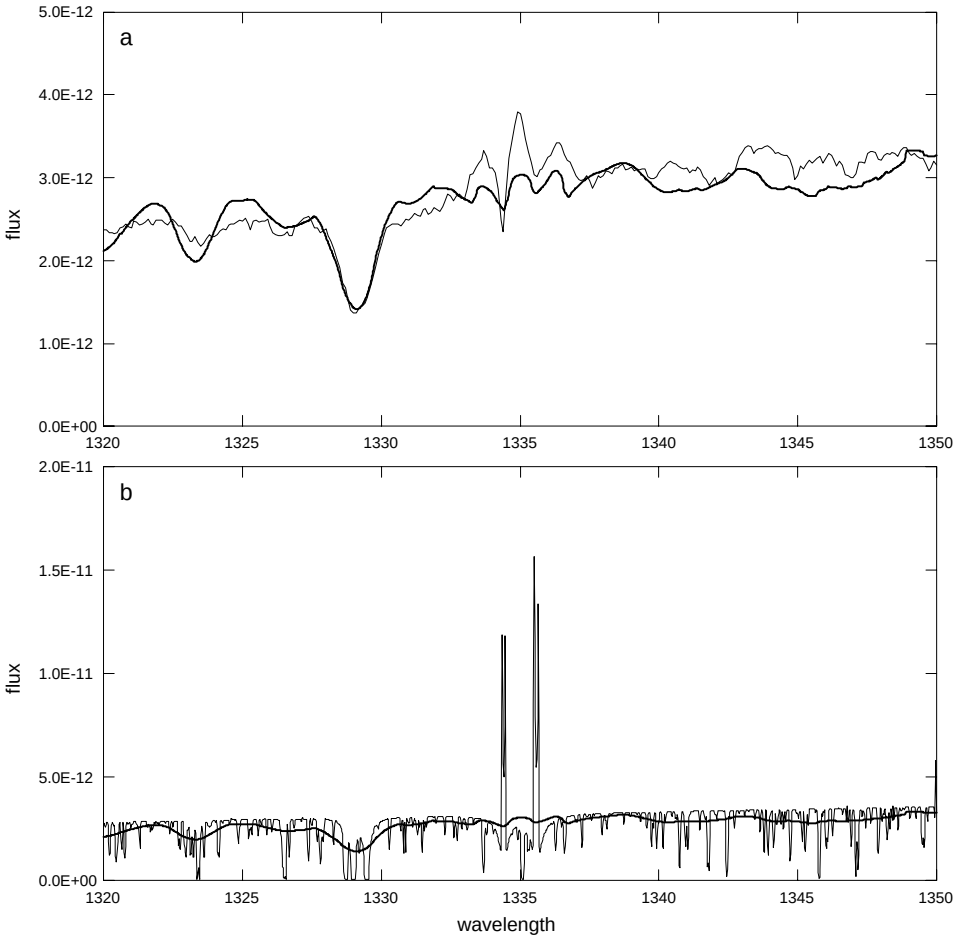

Fig. 4a and b. Flux generated by model CG in the range (1320–1350 Å). **a** flux with rotation (V sin i = 240 km s^{-1}) compared to observations of α Aql (same units as Fig. 1). **b** Comparison of fluxes with rotation (thick line) and without rotation (thin line).

profile comes closer to the observations, but the chromospheric emission is still too weak. P20 and P25 (Figs. 7c and 7d) produces the best fit of the C II multiplet among these four models, with the presence of three peaks, and a global intensity slightly higher than that of the observed profile. Since it is likely that some interstellar absorption occur, as will be discussed in the next section, P20 and P25 are the best candidates among "P" models for the chromosphere of Altair.

4. Models for α Aql with carbon interstellar absorption

Considering the C II multiplet profiles emitted by our five different models (Figs. 4 and 7), it appears that none of them presents any dip as narrow as those of the observed profile. This is due to the high rotation velocity of α Aql, which smoothes out such narrow features. Thus, the observed profile cannot be explained without the help of interstellar absorption.

4.1. Carbon interstellar absorption for model P25

For a first estimation of the carbon interstellar absorption, we consider the model P25, which yields an approximate fit for the Lyman-α line, and an intensity slightly higher than observations in the C II multiplet (model P20 could also be used for the same purpose).

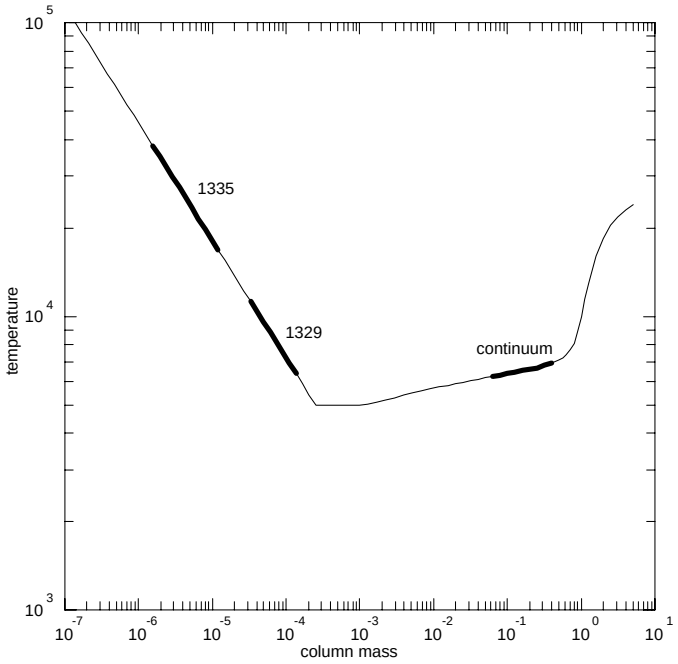

Fig. 5. Variation of temperature vs. column mass for model CG. The regions of formation are indicated for the continuum and the line cores of the two principal multiplets (C I 1329 Å and C II 1335 Å).

For consistency, we keep the hydrogen interstellar column: $\log n_H$ = 18.5. However, there remain (at least) 4 parameters which need to be specified:

- the abundance ratios (C I/H) and (C II/H),
- the Doppler dispersion velocity b (we assume a common value for C I and C II IS clouds),
- the radial velocity of the clouds v_R.

Concerning the radial velocity, it appears that the value of -25 km s^{-1} used for IS hydrogen may be kept for both C I and C II absorptions (this value is practically equal to the radial velocity of the star). The three other parameters are adjusted by trial and error. A relatively good fit is found for the following values: (C I/H) = 5×10^{-5}, (C II/H) = 3×10^{-5} and b = 50 km s^{-1}. The comparison with observations is represented in Fig. 8.

The value of (C I/H)+(C II/H) so obtained for the IS medium is $\approx 10^{-4}$, i. e. 3 or 4 times lower than that corresponding to the cosmic carbon abundance (8.5, cf. Allen 1973). This "depletion factor" of about 0.3 for carbon in the IS medium is in good agreement with the value given by Jenkins (1987). However, the Doppler dispersion velocity b = 50 km s^{-1} of the IS absorption seems to be rather high, even taking into account the presence of 3 cloud systems separated by 7 km s^{-1} (Ferlet et al. 1986).

The fit of the C II multiplet by model P25 is acceptable whereas the computed peaks are somewhat higher than the observed ones. It is possible to improve this fit by using more refined models, as is shown below.

Table 4. Chromospheric models R1 and R2 for α Aql

R1		R2		R1		R2	
$\log m$	T	$\log m$	T	$\log m$	T	$\log m$	T
-6.00	99999	-6.00	99999	-4.58	11710	-4.60	10220
-5.97	88240	-5.96	85862	-4.55	10194	-4.58	9224
-5.94	77182	-5.92	72749	-4.52	8874	-4.55	8501
-5.91	67253	-5.89	61268	-4.49	7725	-4.46	8046
-5.88	58547	-5.85	51520	-4.46	6749	-4.36	7799
-5.85	50968	-5.81	43323	-4.43	5972	-4.27	7653
-5.82	44371	-5.78	36557	-4.40	5438	-4.17	7541
-5.79	38627	-5.74	31246	-4.30	5142	-4.08	7430
-5.76	33726	-5.70	27529	-4.20	5028	-3.98	7320
-5.73	29756	-5.61	25265	-4.10	5000	-3.89	7202
-5.70	26887	-5.51	24075	-4.00	5000	-3.79	7055
-5.60	25064	-5.42	23393	-3.90	5000	-3.70	6851
-5.50	24038	-5.32	22877	-3.80	5000	-3.65	6583
-5.40	23393	-5.22	22372	-3.70	5000	-3.60	6266
-5.30	22877	-5.13	21878	-3.60	5000	-3.55	5935
-5.20	22372	-5.04	21395	-3.50	5000	-3.50	5621
-5.10	21878	-4.94	20859	-3.40	5000	-3.45	5355
-5.00	21395	-4.84	20151	-3.30	5000	-3.40	5164
-4.90	20844	-4.75	19102	-3.20	5000	-3.32	5054
-4.80	20076	-4.72	17694	-3.10	5000	-3.24	5011
-4.70	18888	-4.70	16042	-3.00	5000	-3.16	5000
-4.67	17265	-4.67	14371			-3.08	5000
-4.64	15357	-4.65	12816			-3.00	5000
-4.61	13451	-4.62	11429				

4.2. A tentative reference model with high rotation velocity

Concerning the best fit for Lα, we have reached the same conclusion as in FF95, i. e. that it is obtained using a temperature plateau near 20000 K and a rotation velocity $V \sin i$ close to 300 km s^{-1}. The model "R1" is intermediate between P20 and P25, but its plateau is not horizontal and some smoothing has been applied. It is represented in Fig. 9, where it is compared to the preceding CG and "P" models. It produces a really good fit of Lα and C II line profiles, as may be seen in Fig. 10. The interstellar carbon abundances used to obtain the best fit in this case are slightly higher than in the case of P25: (C I/H) = 6×10^{-5} and (C II/H) = 4×10^{-5}.

4.3. Another model with standard rotation velocity

The good fit obtained with model R1 is restricted to the assumption of high rotation velocity. If we use the standard velocity ($V \sin i$ = 240 km s^{-1}), as measured in most photospheric lines, the Lα profile emitted by model R1 is too narrow (similar to that produced by P25 in Fig. 6d). In FF95, we suggested that this excess rotation velocity was due to an extended chromosphere, principally located in the equatorial region of the star. However, this assumption may raise some objections, since it implies strong differential motions and perhaps stability problems in the atmosphere of the star. So, we tried to find some alternative solution to broaden the Lα line, without changing too much the intensities in carbon lines. This may be done by adding to R1 a low temperature plateau (7000 to 8000 K), in order to broaden the feet of the Lα profile, and slightly reducing the 20000 K plateau, to balance the increase of intensity produced by these low temperature layers. This operation is illustrated by Fig. 11, and the resulting line profiles are represented in Fig. 12. The fit is not so good as for model R1, but nevertheless compatible with observations.

The temperature variations in the chromosphere of the two "R" models are given in Table 4.

Other phenomena may be invoked to explain the apparent excess broadening in Lα. In the case of the Sun, where rotation broadening is negligible, the observed Lα profile is much broader than that computed from standard models (e.g. Vernazza et al. 1981). This property is often attributed to the existence of turbulent motions. For instance, Gouttebroze et al. (1978) pointed out that, to fit the observed profiles, it was necessary to add a *macroturbulent* velocity of about 30 km s^{-1} for Lα and 20 km s^{-1} for Lβ. In the meantime, Fontenla et al. (1991, 1993) computed hydrogen line profiles, taking into account the effects of ambipolar diffusion in the chromosphere-corona transition region. The Lα profiles obtained with ambipolar diffusion were somewhat broader than those of Vernazza et al. (1981), but nevertheless too narrow to match the observations.

Finally, the chromospheric models with high rotation velocity (300 km s^{-1}) yield the best fit for Lα line profiles, but the question of the reality of this high velocity remains open. Further theoretical investigations and, above all, better observations will be necessary to conclude on this point.

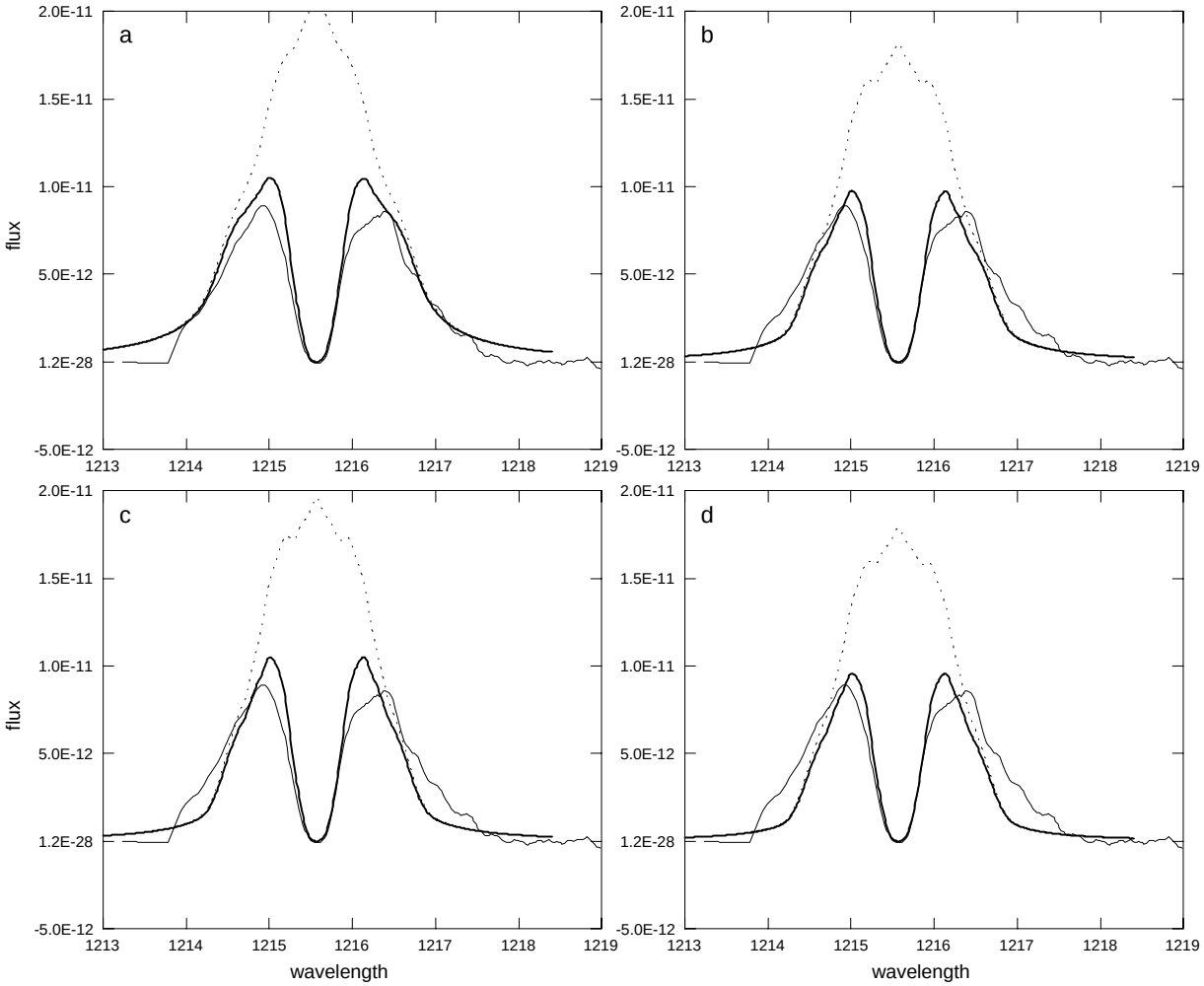

Fig. 6a–d. Lα profiles generated by the different models of α Aql with temperature plateau (same units as Fig. 1). Thin line: observations; dotted line: computed profile without IS absorption; thick line: the same with IS absorption. **a** model P10. **b** P15. **c** P20. **d** P25.

5. Models for α Cep

Since α Cep is more distant than α Aql, its flux at earth is lower (by a factor of about 5), and consequently the relative noise is more important. In addition, the quantity of IS matter along the line of sight is larger ($\log n_H \approx 19.0$ instead of 18.5, cf. Marilli et al., 1997), so that the diagnostic is more uncertain.

We use the same procedure as for α Aql. The Barnes and Evans relation yields $(R/d) = 3.6 \times 10^{-9}$ for α Cep. If the distance is 14.7 pc, the radius is about $2.3 R_\odot$. The rotation velocity retained is $v \sin i$ = 250 km s^{-1}. As for α Aql, the surface gravity is not known with precision, so that we keep the mean value $\log g = 4.0$, which is also the value given by Malagnini & Morossi (1990). With the abovementioned value of (R/d), the model ($T_{eff} = 8000\,K, \log g = 4.0$) of Kurucz (1979) produces a continuum in the range (1320–1350 Å), which is slightly lower than the observed one. The photosphere adopted for α Aql (Table 2) yields a continuum slightly higher than the observations of α Cep. Finally, we obtain the best fit by lowering the temperatures of Table 2 by an amount of 30 K, while keeping constant the values of $\log m$ (Fig. 13). Microturbulent velocities are still fixed to 5 km s^{-1}.

Once taken into account the different value of (R/d) for α Aql and α Cep, it appears that the chromospheres of the two stars are very similar. The surface flux in Lα is slightly lower for α Cep. We find that, to transform a chromospheric model for α Aql into a model for α Cep, it is sufficient to shift the $T(m)$ function by a quantity of -0.1 in $\log m$. For instance, with a plateau at 10000 K, the transition between the temperature minimum and the plateau will be centered at $\log m = -4.05$ for α Cep instead of -3.95 for α Aql. In the same way, for 15000 K, the transition will be centered at $\log m = -4.45$ instead of -4.35, for 20000 K, at -4.65 instead of -4.55, and for 25000 K, at -4.75 instead of -4.65.

Concerning the carbon line range, the conclusions are the same as for α Aql. The model with a plateau at 10000 K produces a pure absorption profile for C II, and thus may be ruled out. The models with plateaux at 15000, 20000 and 25000 K produce C II profiles with peaks and dips located approximately at the same place as in observations, but the peak intensities of the coolest model are too low. The models at 20000 and 25000 K yield, in

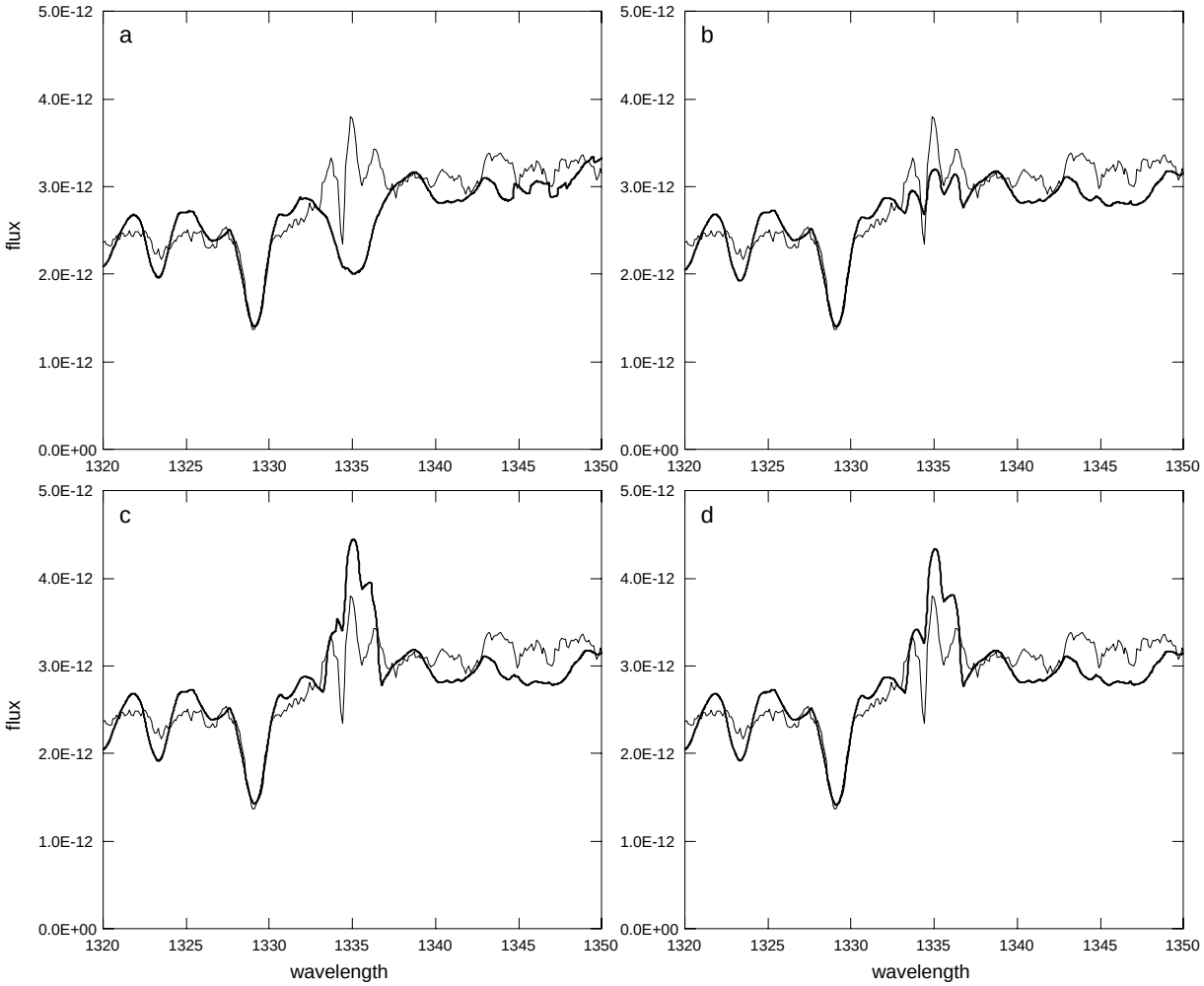

Fig. 7a–d. Fluxes in the C II spectral range for the different models of α Aql with temperature plateau (same units as Fig. 1). Thick line: computation; thin line: observation. **a** model P10. **b** P15. **c** P20. **d** P25.

the absence of IS absorption, peak intensities which are slightly higher than observed.

In order to construct a provisional reference model for α Cep, we use the same procedure as for the "P" models, shifting the chromospheric temperature curve of model R2 by an amount of -0.1 in $\log m$. The model "R3" so obtained is represented in Fig. 14.

As in the case of α Aql, the absorption features are too narrow to be of pure stellar origin. Keeping $\log n_H = 19.0$ (from the analysis of the IS Lα absorption feature), we try to fit the observed C I and C II multiplet profiles by adjusting the abundance ratios, dispersion and radial velocities. One of the best fits is obtained for the following values: (C I/H) = 4×10^{-5}, (C II/H) = 2×10^{-5}, b = 80 km s^{-1} and v_R = -10 km s^{-1}. These abundance values are still compatible with the carbon cosmic abundance, the carbon depletion factor being about 0.2, i.e. slightly lower than for the line of sight of α Aql. The higher value of b, with respect to α Aql, may be the result of a larger number of different IS clouds along the line of sight, in relation with the α Cep to Sun distance.

Fluxes computed from model R3, including IS absorption, are compared to observations in Fig. 15. The fit is relatively good, considering the low signal-to-noise ratio in Lα observations, so that it does not seem useful to try to refine the model.

6. Conclusions

We have studied some simple chromospheric models for α Aql and α Cep, based on high resolution observations of the hydrogen Lyman-α line by the IUE and carbon multiplets by the GHRS/HST. Concerning α Aql, the main improvement with respect to our previous modelling (FF95) consists of the inclusion of the carbon lines in the diagnostic. In this way, we have shown that some models of chromosphere with emitting matter near 10000 K, producing a rather good fit of the observed Lα emission, were unable to explain the C II emission. On the contrary, models with a concentration of matter at a temperature close to 20000 K may produce a rather good fit of both Lα and C II lines, provided that some interstellar absorption is included.

Once this "high temperature" emission established, we reach the same conclusion as FF95, i.e. that the best fit

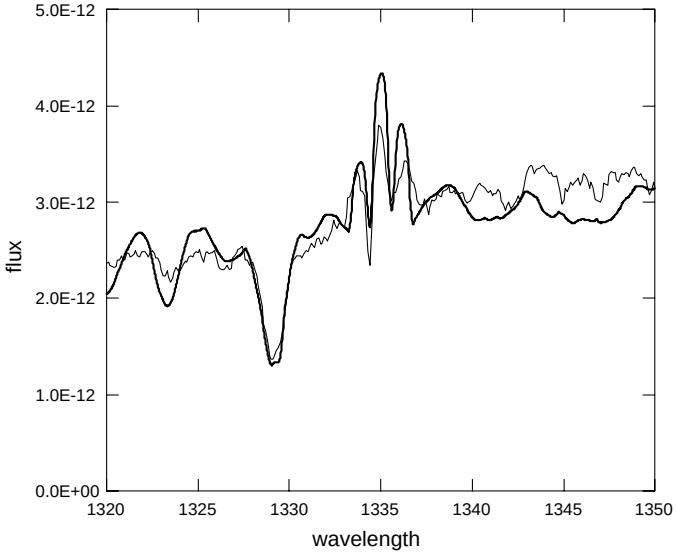

Fig. 8. Fluxes in the carbon spectral range for model P25 with interstellar absorption, compared to observations of α Aql (same units as Fig. 1). Thick line: computation; thin line: observation. IS absorption parameters: (C I/H) = 5×10^{-5}, (C II/H) = 3×10^{-5}, b = 50 km s^{-1} and v_R = -25 km s^{-1}.

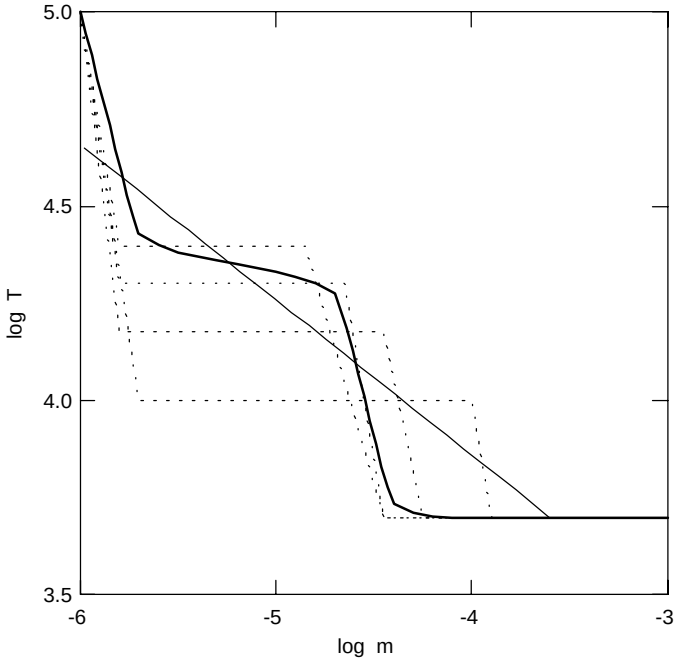

Fig. 9. Variations of temperature (K) vs. column mass (g cm^{-2}) for different chromospheric models of α Aql. Dotted lines: models P10, P15, P20 and P25. Thin solid line: model CG. Thick solid line: model R1.

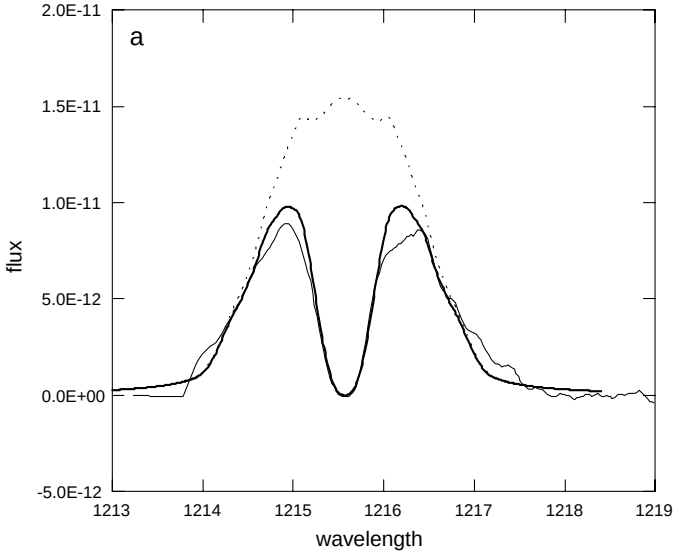

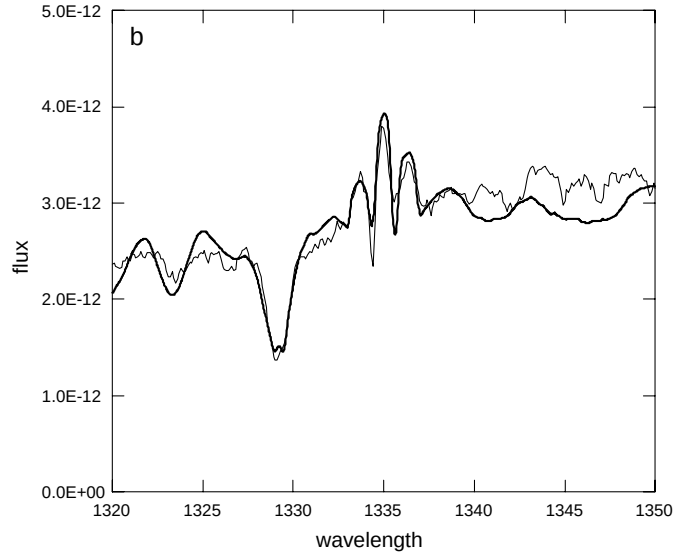

Fig. 10a and b. Fluxes emitted by the model R1 with high rotation velocity ($V \sin i$ = 300 km s^{-1}), compared to observations of α Aql (same units as Fig. 1). Thin solid line: observations. Dotted line (Lα only): computed profile without IS absorption. Thick solid line: computed profile with IS absorption. The IS absorption parameters are: (C I/H) = 6×10^{-5}, (C II/H) = 4×10^{-5}, b = 50 km s^{-1} and v_R = -25 km s^{-1}.

for the Lα line requires a rotation velocity ($v \sin i$ = 280–300 km s^{-1}) higher than that deduced from photospheric lines (220–250 km s^{-1}). This may be due to a concentration of Lα emission in the equatorial region of the star.

However, other broadening processes may be invoked for Lyman-α. The addition of cooler matter in the (7000–8000 K) temperature range reduces the gap between computation and observation but the fitting is not so good as that produced by the high rotation velocity. Other mechanisms, such as macroturbulence or ambipolar diffusion, should be investigated. Better Lα observations would also be necessary to give a reliable interpretation of this excess line broadening.

The weaker emissions of α Cep, with respect to α Aql, which may be observed both in the Lα line and in the C II multiplet, may be explained by a difference of thickness of the chromospheres rather than a difference of temperature. This difference corresponds to a shift of the temperature plateau $\Delta(\log m) = 0.1$, i.e. to a thickness ratio [m(α Cep) / m(α Aql)] $\sim$ 0.8. So, the chromospheres of the two stars are prob-

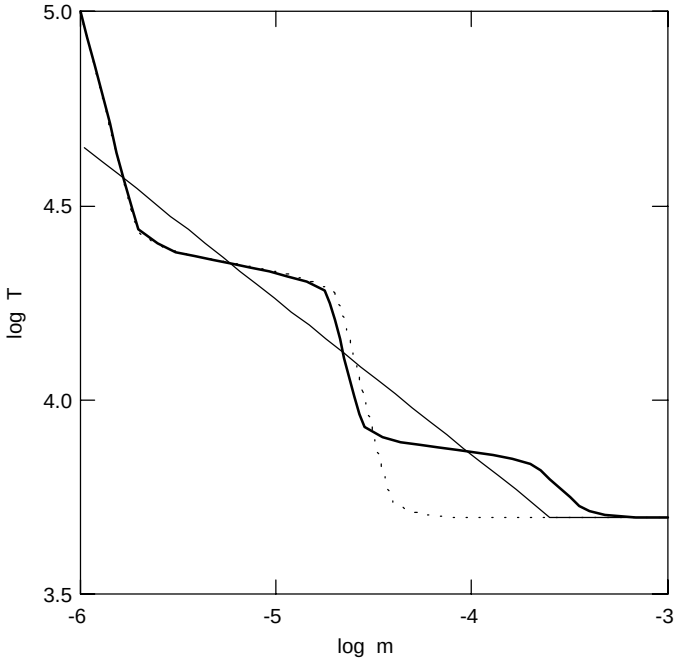

Fig. 11. Variations of temperature (K) vs. column mass ($\mathrm{g\,cm^{-2}}$) for different chromospheric models of α Aql. Thin solid line: model CG. Dotted line: model R1. Thick solid line: model R2.

ably very similar, whereas the C II emission of α Cep is much less evident, mainly as a consequence of a stronger interstellar absorption.

In the context of the onset of convection, α Aql is a particularly interesting star since it might have, as an effect of fast rotation, an equatorial region of type F (convective) and polar regions of type A (radiative). An essential parameter for further modelling of α Aql would be the knowledge of its period of rotation, in order to determine its structure under the joint effects of gravity and centrifugal force. If the chromosphere of α Aql is inhomogeneous, this period of rotation could be determined by a continuous monitoring of its emissions in Lα, C II or other chromospheric lines.

Our models include a chromosphere-corona transition region, but this one is rather arbitrary, since both Lα and C II lines are weakly sensitive to its precise structure. We plan to improve the models in this region of the atmosphere with the help of observations of N V and Si III lines recently obtained by Simon & Landsman (1997).

We also plan to pursue this work by a modelling of the chromospheres of several stars whose Lα emissions have been measured by Marilli et al. (1997): γ Boo, ι U Ma, α Hyi, β Tr A and β Cas.

Acknowledgements. We are grateful to T. Lanz for supplying us with Hα observations and to P. Lemaire for communicating C II solar profiles from the SOHO/SUMER experiment. We also thank the referee for many helpful suggestions, especially concerning stellar models with two plateaux. Non-LTE model atmosphere computations were performed using the facilities of "Institut du développement et des ressources en informatique scientifique" (IDRIS).

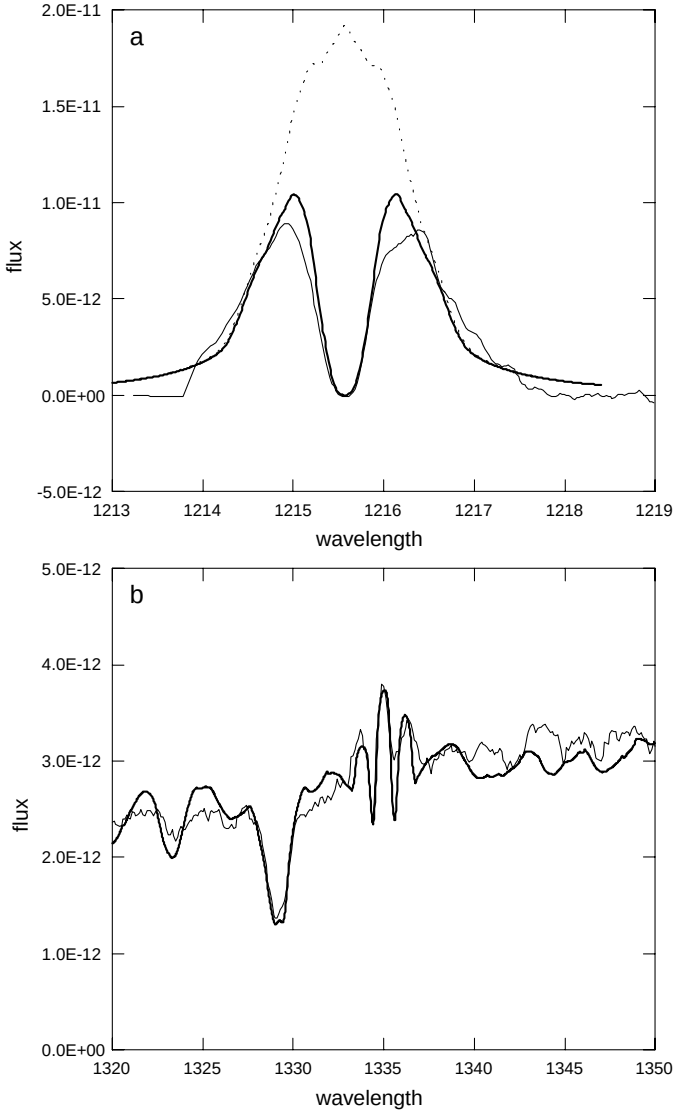

Fig. 12a and b. Fluxes emitted by the model R2 with standard rotation velocity ($V \sin i$ = 240 $\mathrm{km\,s^{-1}}$), compared to observations of α Aql (same units as Fig. 1). Thin solid line: observations. Dotted line (Lα only): computed profile without IS absorption. Thick solid line: computed profile with IS absorption (same IS absorption parameters as for Fig. 10).

Appendix A: radiative transfer in overlapping multiplets with approximate partial redistribution

The two multiplets of C I and C II studied in this paper include overlapping lines which cannot be treated independently. Instead of using an iterative procedure whose convergence might be uncertain, we treat each multiplet as a single line. To this purpose, we define composite absorption coefficients and source functions as follows.

Let i and j be the indexes of the lower and upper levels of a transition, respectively; k indicates a sublevel of i and l a sublevel of j. The absorption coefficient for the whole multiplet is, as a function of frequency:

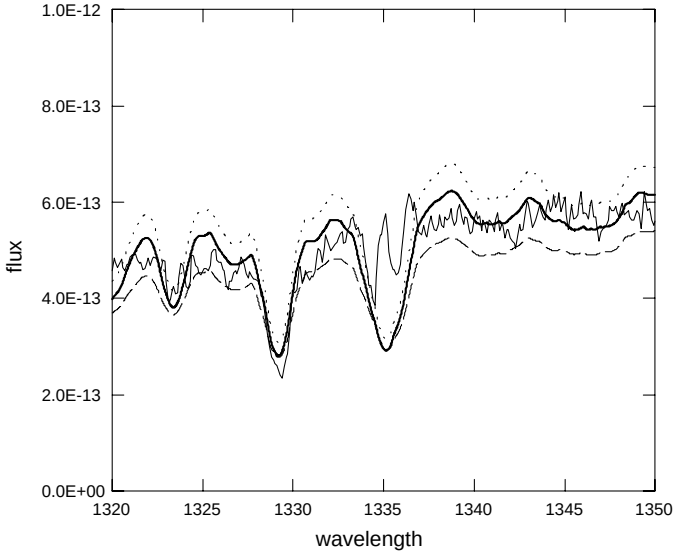

Fig. 13. Fluxes in the carbon spectral range emitted by α Cep, compared to models without chromosphere (same units as Fig. 1). Thin solid line: observations; dashed line: model (8000, 4.0, 0) of Kurucz (1979); dotted line: same model as for α Aql (Table 2); thick solid line: chosen model (temperatures of Table 2 lowered by 30 K).

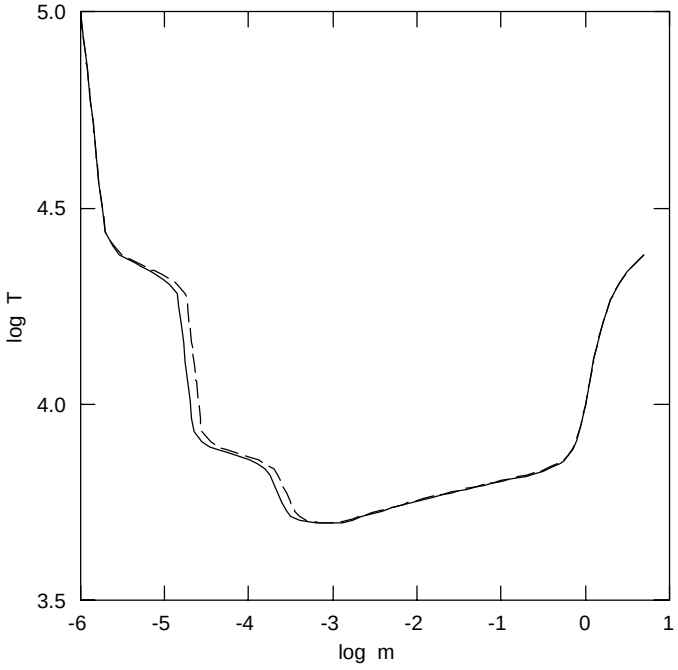

Fig. 14. Variations of temperature (K) vs. column mass (g cm^{-2}) for models R3 (α Cep, solid line), compared to model R2 (α Aql, dashed line).

$$\kappa_{ij}(\nu) = \sum_k \sum_l \kappa_{ikjl}(\nu) \tag{A1}$$

where κ_{ikjl} is the absorption coefficient for the subtransition (ik, jl):

$$\kappa_{ikjl}(\nu) = \frac{c^2}{8\pi\nu_{ikjl}^2}\left(n_{ik}\frac{g_{jl}}{g_{ik}} - n_{jl}\right) a_{jlik}\,\phi_{ikjl}(\nu) \tag{A2}$$

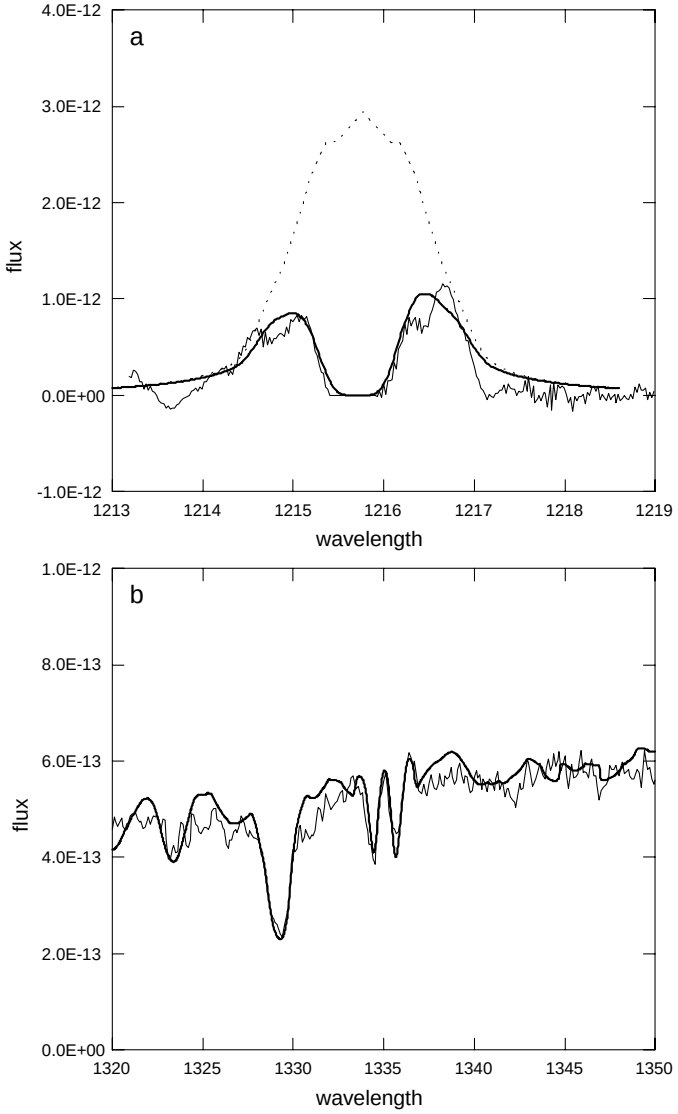

Fig. 15a and b. Fluxes emitted by the model R3 compared to observations of α Cep (same units as Fig. 1). Thin solid line: observations. Dotted line (Lα only): computed profile without IS absorption. Thick solid line: computed profile with IS absorption. The IS absorption parameters are: $n_H = 10^{19}$, (C I/H) = 4×10^{-5}, (C II/H) = 2×10^{-5}, b = 80 km s^{-1} and v_R = -10 km s^{-1}.

(ν_{ikjl}: frequency of the subtransition; n_{ik}, n_{jl}: populations of sublevels; g_{ik}, g_{jl}: statistical weights of sublevels; a_{jlik}: Einstein coefficients for spontaneous emission). The normalized profile $\phi_{ikjl}(\nu)$ is:

$$\phi_{ikjl}(\nu) = \frac{1}{\sqrt{\pi}\Delta\nu_D} H\left(\frac{\Gamma_{ikjl}}{4\pi\Delta\nu_D}, \frac{|\nu - \nu_{ikjl}|}{\Delta\nu_D}\right) \tag{A3}$$

($\Delta\nu_D$: Doppler width; H: Voigt function; Γ_{ikjl}: damping rate).

We assume that the populations of the different sublevels of the same level are proportional to their statistical weights:

$$\frac{n_{i1}}{g_{i1}} = \frac{n_{i2}}{g_{i2}} = ... = \frac{N_i}{G_i} \tag{A4}$$

(N_i, G_i: population and statistical weight of the global level i).

In addition, we neglect the differences of frequency between the subtransitions ($\nu_{ikjl} \approx \nu_{ij}$). Combining the preceding equations, we obtain:

$$\kappa_{ij}(\nu) = \frac{c^2}{8\pi\nu_{ij}^2}\left(N_i\frac{G_j}{G_i} - N_j\right) A_{ji}\,\phi_{ij}(\nu) \tag{A5}$$

with:

$$A_{ji} = \frac{1}{G_j}\sum_k\sum_l g_{jl}\,a_{jlik} \tag{A6}$$

and:

$$\phi_{ij}(\nu) = \frac{\sum_k\sum_l g_{jl}\,a_{jlik}\,\phi_{ikjl}(\nu)}{G_j A_{ji}} \tag{A7}$$

By adding the emission coefficients of the different subtransitions, we obtain the source function of the multiplet:

$$S_{ij}(\nu) = \frac{\sum_k\sum_l \kappa_{ikjl}(\nu)S_{ikjl}(\nu)}{\kappa_{ij}(\nu)} \tag{A8}$$

where S_{ikjl} is the source function of a subtransition:

$$S_{ikjl}(\nu) \;=\; \epsilon_{ikjl}B_{ikjl} + \frac{1-\epsilon_{ikjl}}{\phi_{ikjl}(\nu)} \times\int_0^\infty R_{ikjl}(\nu',\nu)J(\nu')d\nu' \tag{A9}$$

(ϵ_{ikjl} and B_{ikjl} are coupling coefficients of the equivalent two-level atom, R_{ikjl} the redistribution function of the subtransition, and J the angle-averaged intensity).

If we assume that the coupling factors are the same for all subtransitions of the same multiplet ($\epsilon_{ikjl} \approx \epsilon_{ij}$, $B_{ikjl} \approx B_{ij}$), we obtain the classical formula for the source function:

$$S_{ij}(\nu) = \epsilon_{ij}B_{ij} + \frac{1-\epsilon_{ij}}{\phi_{ij}(\nu)}\int_0^\infty R_{ij}(\nu',\nu)J(\nu')d\nu' \tag{A10}$$

with the composite redistribution function:

$$R_{ij}(\nu',\nu) = \frac{1}{G_j A_{ji}}\sum_k\sum_l g_{jl}\,a_{jlik}\,R_{ikjl}(\nu',\nu) \tag{A11}$$

With the help of formulae (8) and (12) we can solve the radiative transfer equation for the whole multiplet in the same way as for a single line. In this paper, we used the Feautrier method for this purpose. Individual redistribution functions R_{ikjl} were calculated according to the approximation of Omont et al. (1972).

References

Allen C.W., 1973, Astrophysical Quantities. 3rd edition, Athlone Press, London

Barnes T.G., Evans D.S., 1976, MNRAS 174, 489

Blanco C., Catalano S., Marilli E., 1980, In: Proceedings of Second European IUE Conf., ESA SP-157, p. 67

Carpenter K.G., Slettebak A., Sonneborn G., 1984, ApJ 286, 741

Catalano S., Gouttebroze P., Marilli E., Freire Ferrero R., 1990, In: Tuominen i., Moss D., Rudiger G. (eds.) Proc. IAU Coll. 130, Helsinki, Finland, Lecture Notes in Physics 380, 466

Catalano S., Marilli E., Freire Ferrero R., Gouttebroze P., 1991, A&A 250, 573

Clark R.E.H., Abdallah Jr. J., Mann J.B., 1991, ApJ 381, 597

Cunto W., Mendoza C., Ochsenbein F., Zeippen C.J., 1993, A&A 275, L5

Ferlet R., Lallement R., Vidal-Madjar A., 1986, A&A 163, 204

Fontenla J.M., Avrett E.H., Loeser R., 1991, ApJ 377, 712

Fontenla J.M., Avrett E.H., Loeser R., 1993, ApJ 406, 319

Freire Ferrero R., Catalano S., Gouttebroze P., Marilli E., 1990, In: Proc. Int. Symp. IUE, Toulouse, France, ESA SP-310, 315

Freire Ferrero R., Catalano S., Marilli E., et al., 1992, In: G.S. Vaiana Memorial Symp., Palermo, Italy, 22-26/6/92

Freire Ferrero R., Gouttebroze P., Catalano S., et al., 1995, ApJ 439, 1011 (FF95)

Gouttebroze P., Lemaire P., Vial J.C., Artzner G., 1978, ApJ 225, 655

Hanbury Brown R., Davis J., Allen L.R., 1974, MNRAS 167, 121

Hanbury Brown R., Davis J., Allen L.R., Rome J.M., 1967, MNRAS 137, 393

Jenkins E.B., 1987, In: Hollenbach D.J., Thronson H.A. Jr. (eds.) Interstellar Processes. Reidel, Dordrecht, p. 533

John T.L., 1988, A&A 193, 189

Johnson L.C., 1972, ApJ 174, 227

Kurucz R.L., 1979, ApJS 40, 1

Kurucz R.L., 1998, line list gf0140.10 from database http://cfaku5.harvard.edu

Lanz T., Catala C., 1992, A&A 257, 663

Lites B.W., Shine R.A., Chipman E.G., 1978, ApJ 222, 333

Lortet M.C., Roueff E., 1969, A&A 3, 462

Malagnini M.L., Morossi C., 1990, A&AS 85, 1015

Marilli E., Catalano S., Freire Ferrero R., Gouttebroze P., 1992, A&A 265, 643

Marilli E., Catalano S., Freire Ferrero R., et al., 1997, A&A 317, 521

Omont A., Smith E.W., Cooper J., 1972, ApJ 175, 185

Shallis M.J., Blackwell D.E., 1980, A&A 81, 336

Simon T., Landsman W.B., 1997, ApJ 483, 435

Simon T., Landsman W.B., Gilliland, R.L., 1994, ApJ 428, 319

Stürenburg S., Holweger H., 1990, A&A 237, 125

Sutton K., 1978, JQSRT 20, 333

Van Regemorter H., 1962, ApJ 136, 906

Vernazza J.E., Avrett E.H., Loeser R., 1976, ApJS 30, 1

Vernazza J.E., Avrett E.H., Loeser R., 1981, ApJS 45, 635

Walter F.M., Matthews L.D., Linsky J.L., 1995, ApJ 447, 353

Wiese W.L., Smith M.W., Glennon B.M., 1966, Atomic Transition Probabilities. Vol. I, NSRDS-NBS 4